

Reflectance and Fluorescence Spectral Recovery via Actively Lit RGB Images

Ying Fu, *Student Member, IEEE*, Antony Lam, *Member, IEEE*, Imari Sato, *Member, IEEE*, Takahiro Okabe, *Member, IEEE*, and Yoichi Sato, *Member, IEEE*

Abstract—In recent years, fluorescence analysis of scenes has received attention in computer vision. Fluorescence can provide additional information about scenes, and has been used in applications such as camera spectral sensitivity estimation, 3D reconstruction, and color relighting. In particular, hyperspectral images of reflective-fluorescent scenes provide a rich amount of data. However, due to the complex nature of fluorescence, hyperspectral imaging methods rely on specialized equipment such as hyperspectral cameras and specialized illuminants. In this paper, we propose a more practical approach to hyperspectral imaging of reflective-fluorescent scenes using only a conventional RGB camera and varied colored illuminants. The key idea of our approach is to exploit a unique property of fluorescence: the chromaticity of fluorescent emissions are invariant under different illuminants. This allows us to robustly estimate spectral reflectance and fluorescent emission chromaticity. We then show that given the spectral reflectance and fluorescent chromaticity, the fluorescence absorption and emission spectra can also be estimated. We demonstrate in results that all scene spectra can be accurately estimated from RGB images. Finally, we show that our method can be used to accurately relight scenes under novel lighting.

Index Terms—Reflectance and Fluorescence Spectra Recovery, Fluorescent Chromaticity Invariance, Varying Illumination

1 INTRODUCTION

FLUORESCENCE analysis has received attention in recent years. This is because fluorescence can provide additional information about scenes and has been applied to problems in camera spectral sensitivity estimation [1], 3D reconstruction [2], [3], immersion range scanning [4], and color relighting [5], [6] to name a few.

Fluorescence is also very different from ordinary reflectance in the way it responds to incident light [7], [8]. When a reflective surface is illuminated at a particular wavelength it reflects back light of the same wavelength. Fluorescent surfaces on the other hand, will absorb incident light at certain wavelengths and then emit back light at longer wavelengths. This wavelength shifting phenomenon is known as Stokes shift [9][10].

As the properties of fluorescence are very different from ordinary reflectance, neglecting fluorescence can result in completely incorrect estimation of photometric properties. This in turn negatively affects many methods that rely on accurate color estimation. We see a scene is captured under blue and green lights (Figure 1(a)). When the effects of fluorescence are considered (Figure 1(b)), the simulated relighting results are close to the ground truth. However, when we assume that the scene does

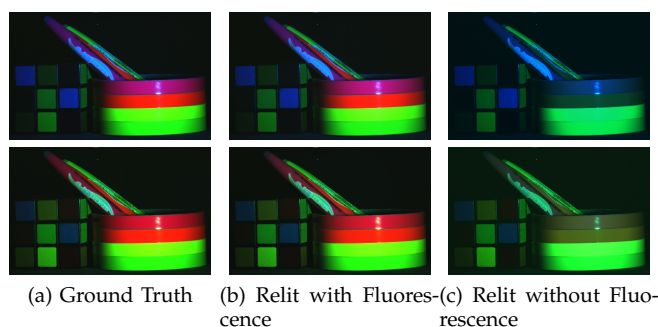


Fig. 1: (a) The scene captured under blue and green light. (b) Simulated relighting results with consideration of fluorescent effects. (c) The relighting results without considering fluorescence.

not include fluorescent materials, the relighting results for the fluorescent materials are wrong (Figure 1(c)).

It is also the case that in practice, most fluorescent objects are not purely fluorescent. Instead, they contain a combination of reflective and fluorescent components so both components need to be considered. These two components can be described in terms of the reflectance, fluorescence absorption and emission spectra. The reflectance spectrum is used to describe how much light is reflected by the reflective component at different wavelengths. The fluorescence absorption and emission spectra on the other hand, describe how much light is absorbed at shorter wavelengths and then emitted at longer wavelengths. Therefore, to capture and recover reflective and fluorescent components, a reflective-fluorescent imaging system needs to be able to recover the reflectance spectrum for the reflective component,

- Y. Fu and Y. Sato are with Institute of Industrial Science, the University of Tokyo, Japan.
E-mail: {fuying, ysato}@iis.u-tokyo.ac.jp
- A. Lam is with Saitama University, Japan.
E-mail: antonylam@cv.ics.saitama-u.ac.jp
- I. Sato is with National Institute of Informatics, Japan.
E-mail: imarik@nii.ac.jp
- T. Okabe is with Kyushu Institute of Technology, Japan.
E-mail: okabe@ai.kyutech.ac.jp

and absorption and emission spectra for the fluorescent component.

The conventional approach to capturing these two components is to exhaustively measure different combinations of reflecting, absorbing and emitting wavelengths [11]. This process is labor intensive and more efficient approaches for imaging scenes is desired. Zhang and Sato [8] proposed a method that uses an RGB camera and independent component analysis (ICA) to separate reflective and fluorescent components but their method does not capture the spectral distributions of reflectance, fluorescence absorption and emission. In recent work, methods for hyperspectral imaging of reflective-fluorescent scenes have been proposed [5], [6]. These methods are effective but require specialized cameras and specialized illuminants such as narrowband light or high frequency light spectra.

We propose a more practical approach to hyperspectral imaging of reflective-fluorescent scenes using only a conventional RGB camera and varied colored illuminants. Our method takes as input RGB images under different lighting and effectively separates reflectance and fluorescence at each wavelength. These separated results can then be used for tasks such as accurate color relighting of scenes under novel lighting (Figure 4).

The key idea in our approach is to exploit a unique property of fluorescence: the chromaticity of fluorescence emissions are invariant under different illuminants. Based on this property, we formulate a method that takes RGB images and performs pixel-wise estimation of spectral reflectance and fluorescent chromaticity. The method works by iteratively improving estimates of the spectral reflectance and fluorescent chromaticity in turn. We show our method is robust to initialization conditions and converges onto accurate spectral reflectance and fluorescent chromaticity for real scenes. Then we propose methods for estimating the fluorescence absorption and emission spectra of the scene given the estimated spectral reflectance data and fluorescent chromaticities.

In summary, our main contributions are that we

- 1) Exploit the illuminant-invariant chromaticity of fluorescence to estimate both spectral reflectance and fluorescent chromaticity from RGB images,
- 2) Devise a means for estimating fluorescence absorption and emission spectra from given spectral reflectance and fluorescent chromaticity,
- 3) Ultimately, presenting the first system capable of imaging all reflectance and fluorescence absorption and emission spectra of real scenes using only a conventional RGB camera and varied colored illuminants.

We show our method is accurate and demonstrate its effectiveness in predicting color relighting of real scenes.

The rest of this paper is organized as follows. Section 2 reviews the related work on estimation methods for reflective and fluorescent components, and fluorescence

applications. In Section 3, we describe the fluorescence model and properties of fluorescent surfaces. Section 4 presents the proposed method based on the properties of fluorescent materials. The experimental results are provided in Section 5. The spectral distributions of our illuminants are detailed in Section 6. Finally, conclusions are drawn and future directions of our research are discussed in Section 7.

2 RELATED WORK

There have been a number of effective methods for estimating the spectral reflectance of scenes. For example, Tominaga [12] recovered reflectance spectra from images captured by a monochrome camera with sequentially placed band-pass filters. Park *et al.* [13] employed multiplexed illumination produced by sets of LEDs for fast spectral imaging of dynamic scenes. Chi *et al.* [14] obtained the spectral information of a scene in the presence of unknown ambient illumination by optimizing wide band filtered illumination. Han *et al.* [15] recovered spectral reflectance using multiple illuminations produced by the color wheel in a DLP projector. Jiang and Gu [16] recovered spectral reflectance from two images taken with conventional consumer cameras under commonly available lighting conditions. These methods are practical and effective for imaging spectral reflectance but their limitation is they cannot accurately capture scenes with fluorescent surfaces. The reason for this loss in accuracy is because reflective and fluorescent surfaces react to incident light very differently.

The detrimental effects of not considering fluorescence is nicely illustrated in Johnson and Fairchild [7] where they showed that taking fluorescence into account dramatically improved color renderings. Lee *et al.* [17] provided a mathematical description for fluorescent processes and recovered the additive spectra of reflective and fluorescent components but did not separate them. Furthermore, Barnard [18] proposed improvements to color constancy algorithms which included spectral data from several fluorescent materials. Later, Wilkie *et al.* [19] showed accurate results by rendering fluorescence emissions using diffuse surfaces that can reflect light at a wavelength different from its incident illuminant wavelength. Hullin *et al.* [20] also demonstrated the importance of modeling different reflective-fluorescent materials by introducing the bidirectional reflectance and reradiation distribution function (BRDF).

A conventional way to measure fluorescence in the spectral domain is to use Bispectral measurements [11]. However, exhaustively measuring different combinations of absorption and emission wavelengths is labor intensive. Later, Zhang and Sato [8] proposed an ICA based reflective-fluorescent separation method. Tominaga *et al.* [21] used two light sources and multispectral imaging to estimate fluorescence emission spectra. Alterman *et al.* [22] separated the appearance of each fluorescent dye from a mixture by unmixing multiplexed images. Fuchs [23] estimated the reflectance and

fluorescence emission spectra of coral. None of these recent methods fully recover all reflective and fluorescent components of scenes.

In recent work, methods for hyperspectral imaging of reflective-fluorescent scenes have been proposed. Lam and Sato [5] provided a method for recovering the full spectral reflectance and fluorescence absorption and emission spectra of scenes but they required a multiband camera and multiple narrowband illuminants. Fu *et al.* [6] also recovered the full spectral reflectance and fluorescence spectra of scenes by using high frequency light spectra but they require a hyperspectral camera and a programmable light source: a device that can be programmed to produce arbitrary light spectra. Zheng *et al.* [24] recovered all the different types of spectra by using 3 ordinary illuminants, but they still require a hyperspectral camera. While effective, all these methods require specialized equipment so their use in applications is limited. We propose a more practical approach to fully capturing the reflectance and fluorescence absorption and emission spectra of scenes using an RGB camera and varied illuminants.

The wavelength shifting phenomenon of fluorescence has also been studied and used for solving computer vision problems. Han *et al.* [1] utilized separated fluorescent components to estimate camera spectral sensitivity under unknown illumination. Sato *et al.* [2] used the fluorescent component for photometric stereo. Treibitz *et al.* [3] constructed 3D models from fluorescence. Hullin *et al.* [4] utilized the fluorescent component for fluorescent immersion range scanning. Lam and Sato [5] and Fu *et al.* [6] predicted the appearance of relit fluorescent scenes after all information of spectra were recovered in the scene. Fu *et al.* [25] removed scene interreflection using fluorescence.

3 REFLECTANCE AND FLUORESCENCE

In this section, we first describe a physical model for reflective-fluorescent scenes. Then, we detail how reflectance and fluorescence spectra can be measured in terms of a physical model. Finally, we explain the illuminant-invariant chromaticity of fluorescence by derivations of the model, which will be employed in our method to simplify our problem for estimating reflectance and fluorescence spectra.

3.1 Reflectance and Fluorescence Model

Most fluorescent materials exhibit both reflectance and fluorescent emission. Since reflectance and fluorescence are different physical processes, they need to be described using different models.

The appearance of a surface point's reflection depends on the incident light and the scene's reflectance. The observed spectrum of an ordinary reflection at wavelength λ can be expressed as

$$p_r(\lambda) = l(\lambda)s(\lambda), \quad (1)$$

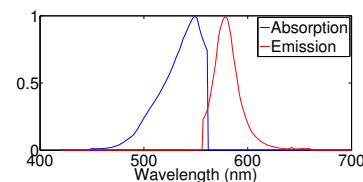


Fig. 2: An example of absorption and emission spectra from the McNamara and Boswell Fluorescence Spectral Dataset [26].

where $l(\lambda)$ is the spectrum of the incident light at wavelength λ and $s(\lambda)$ is the spectral reflectance of the material at wavelength λ .

Fluorescence typically transfers the energy from one wavelength to a longer wavelength. Fluorescent emission occurs after an orbital electron of a molecule, atom or nanostructure absorbs light and is excited, then the electron relaxes to its ground state by emitting a photon of light and releasing heat after several nanoseconds. The higher the light frequency is, the more energy the light carries. Since some of the absorbed energy is lost as heat, the fluorescent emission will be shifted to longer wavelengths. How much light is absorbed at different wavelengths and then emitted is described by the absorption and emission spectra. Figure 2 shows an example of such spectra for a fluorescent material over the visible spectrum. The observed spectrum of a pure (non-reflective) fluorescent surface depends on the incident light, absorption spectrum and emission spectrum of the material [8], and can be described as

$$p_f(\lambda) = \left(\int l(\lambda')a(\lambda')d\lambda' \right) e(\lambda), \quad (2)$$

where λ' and λ are the wavelengths of the incident light and the outgoing fluorescence, respectively. $l(\lambda')$ is the illuminant intensity at wavelength λ' , $a(\lambda')$ is the normalized absorption spectrum and $e(\lambda)$ represents the emission spectrum.

3.2 Reflectance and Fluorescence Capture Process

We begin by briefly describing how reflectance and fluorescence absorption and emission spectra for a single point can be measured using bispectral measurements [11].

Reflectance Measurement: Stokes shift indicates that a fluorescent point illuminated at wavelength λ' will generally emit light at longer wavelengths λ . The implication is that light will not generally emit at the same wavelength as the illuminant. Thus if we illuminate a reflective-fluorescent point at wavelength λ' and observe the point at wavelength λ when $\lambda' = \lambda$, we will observe only the reflective component¹. An example of reflectance only recovery can be seen in Figure 3(a). In this

1. There is usually an overlap between the long wavelength end of the absorption spectrum and the short wavelength end of the emission spectrum (Figure 2). This would cause the observed light at the "overlap wavelengths" to be a mix of reflectance and emission. However, in our case, the reflected light is typically much brighter than the emission and so cross-talk is minimal [27].

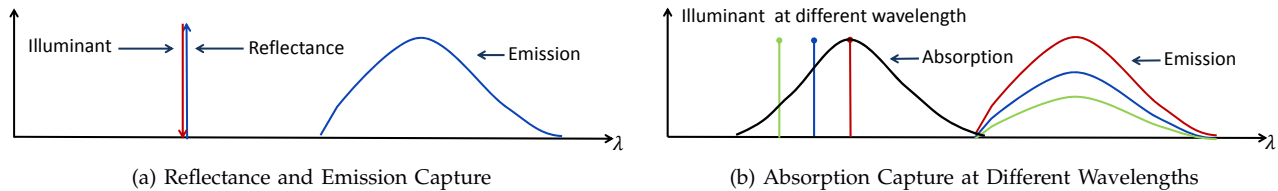


Fig. 3: Capture of reflective-fluorescent spectra at a single point in a scene. (a) When the reflective-fluorescent scene is illuminated, the reflectance spectrum can be measured at the same wavelength as the illuminant while the emission spectrum can be captured at longer wavelengths. (b) Varying the illuminant over different wavelengths and measuring the fluorescence emission spectrum at the same wavelength. The observation of different scaled emissions allow us to infer the fluorescence absorption each wavelength.

case, the scene is illuminated by narrowband illuminants across the visible spectrum in 10 nm intervals from 400 nm to 700 nm. The reflectance spectrum is captured by observing the same wavelength as the illuminant. In the overlapping region between the absorption and emission spectra, we still observe the reflectance spectrum clearly since the fluorescent emission there is extremely weak.

Emission Measurement: An emission spectrum will maintain the same shape regardless of the illuminant. The only effect an illuminant has on the observed emission spectrum is its scale. Since Stokes shift causes emissions to be observed at longer wavelengths than the illuminant, we could fix an illuminant at λ' and observe the emission for all wavelengths $\lambda > \lambda'$. As long as we set λ' at a short enough wavelength, we can observe the entire emission spectrum. In the case of a reflective-fluorescent point, no reflectance would be observed at λ as reflectance only occurs at the same wavelength as the illuminant. Figure 3(a) shows an emission illuminated by a narrowband light.

Absorption Measurement: The absorption spectrum is just defined as how much the illuminant scales the emission at a given wavelength. Thus we can simply observe the scale of the emission at a wavelength λ while varying the illuminant wavelength λ' for $\lambda' > \lambda$. How much the strength of the observed emission changes at wavelength λ defines the absorption spectrum at wavelength λ' . Figure 3(b) shows the observation of different scaled emissions for inferring absorption at the illuminant wavelength.

In our paper, we use bispectral measurements to obtain the ground truth to evaluate the accuracy of our method.

3.3 Constant Chromaticity

From Equation (2), we can see that for a given fluorescent material, its emission spectrum always has the same spectral distribution regardless of the illuminant's spectral distribution (Figure 3(b)).

Thus when a pure fluorescent surface is captured by an RGB camera, the color of the pixel for the n -th channel under the m -th illuminant is

$$\begin{aligned} f_n^m &= \int c_n(\lambda) p_f^m(\lambda) d\lambda \\ &= \left(\int l_m(\lambda') a(\lambda') d\lambda' \right) \int c_n(\lambda) e(\lambda) d\lambda. \end{aligned} \quad (3)$$

Here, $c_n(\lambda)$ ($n = (r, g, b)$) is the camera spectral sensitivity for the R, G, and B channels. Let

$$D_n = \int c_n(\lambda) e(\lambda) d\lambda, \quad (4)$$

be called the reference value of the emission spectrum $e(\lambda)$.

We can see that $\int l_m(\lambda') a(\lambda') d\lambda'$ is determined by the absorption spectrum and incoming illumination spectrum, and independent from the spectrum of the outgoing fluorescence. Replacing this part by k_m and substituting Equation (4) into (3), Equation (3) can be rewritten as

$$f_n^m = k_m D_n. \quad (5)$$

Note that k_m is the same for all three channels.

Then the chromaticity E_n^m of the fluorescent component for the n -th channel under the m -th illuminant becomes

$$E_n^m = \frac{k_m D_n}{\sum_{t=1}^3 k_m D_t} = \frac{D_n}{\sum_{t=1}^3 D_t} = E_n, \quad (6)$$

where E_n is called the reference chromaticity. The scale factor k_m can be eliminated, thus the chromaticity of the fluorescent material is independent of both the illuminant and absorption spectrum, and it only depends on the camera spectral sensitivity and emission spectrum. Equation (6) implies chromaticity value E_n^m is constant under varying illuminations. We also note that since $\sum_{n=1}^3 E_n = 1$, $E_3 = 1 - E_1 - E_2$, the chromaticity can be uniquely expressed with only 2 values. However, for convenience in our derivations, we will express chromaticity in terms of 3 values.

4 REFLECTANCE AND FLUORESCENCE SPECTRA ESTIMATION

In this section, we present a method to recover the full spectra of reflectance and fluorescence. First, the reflectance spectrum and the chromaticity of the fluorescent component are estimated in an alternating optimization process with an initialization of the fluorescent chromaticity. Then, the fluorescence absorption and emission spectra are recovered. Finally, we discuss how the fluorescent chromaticity can be initialized in our method.

Throughout this paper, we use bold uppercase letters (e.g., \mathbf{W}), bold lowercase letters (e.g., \mathbf{s}) and plain

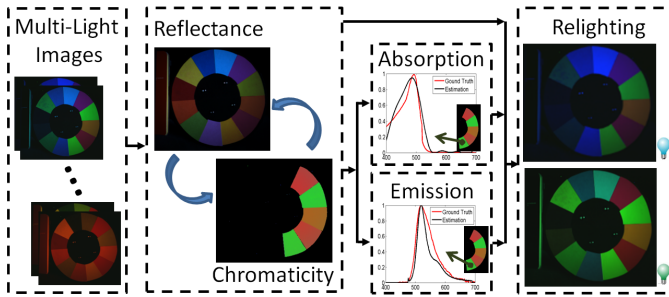


Fig. 4: Overview of the method. The input images are captured under varied illuminants. The reflectance spectrum and the chromaticity of the fluorescent component are optimized in a process of alternating iterations that exploits the illuminant-invariant chromaticity of fluorescence. After that, the fluorescence absorption and emission spectra are estimated. All these recovered spectra can be used to relight the reflective-fluorescent scene under new illuminants.

lowercase or uppercase letters (e.g., s and E) to denote matrices, column vectors, and scalars, respectively.

4.1 Problem Formulation

We start by describing the basic formulation of our problem. When taking an image of a scene with reflective-fluorescent components using an RGB camera, the intensity of each pixel for the n -th channel under the m -th illuminant is

$$p_n^m = r_n^m + f_n^m. \quad (7)$$

r_n^m is the reflective component for the n -th channel under the m -th illuminant and can be described by

$$r_n^m = \int c_n(\lambda) l_m(\lambda) s(\lambda) d\lambda, \quad (8)$$

where $s(\lambda)$ is the spectral reflectance of the material at wavelength λ , $l_m(\lambda)$ is the m -th illuminant's intensity and $c_n(\lambda)$ ($n = 1, 2, 3$) is the corresponding camera spectral sensitivity for the R, G, and B channels.

Substituting Equations (8) and (3) into Equation (7),

$$p_n^m = \int c_n(\lambda) l_m(\lambda) s(\lambda) d\lambda + \left(\int l_m(\lambda') a(\lambda') d\lambda' \right) \int c_n(\lambda) e(\lambda) d\lambda. \quad (9)$$

Equation (9) describes how the components of a reflective-fluorescent surface jointly appear in a camera image under illuminant l_m . Our task is to determine the full spectral reflectance s and fluorescence absorption spectrum a and emission spectrum e given the observed p_n^m under different illuminants l_m and camera spectral sensitivity c_n , which can be estimated by

$$\{\hat{s}, \hat{a}, \hat{e}\} = \arg \min_{s, a, e} G(s, a, e), \quad (10)$$

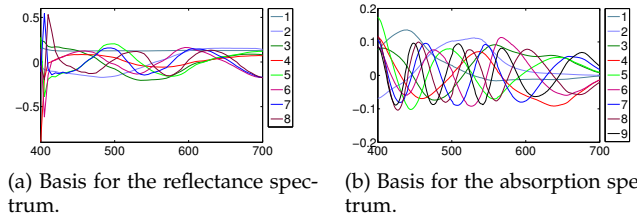


Fig. 5: The bases are used to describe (a) reflectance and (b) fluorescence absorption spectra.

where

$$G(s, a, e) = \sum_m \sum_n \|p_n^m - \hat{p}_n^m(s, a, e)\|_2^2 = \sum_m \sum_n \left\| \int p_n^m - c_n(\lambda) l_m(\lambda) s(\lambda) d\lambda - \left(\int l_m(\lambda') a(\lambda') d\lambda' \right) \int c_n(\lambda) e(\lambda) d\lambda \right\|_2^2 \quad (11)$$

and $\hat{p}_n^m(s, a, e)$ is the estimated parameterization of p_n^m .

Our method for optimizing Equation (10) makes use of the illuminant-invariant chromaticity property of fluorescence. Therefore, all spectral components can be determined in two stages. We start by using the illuminant-invariant chromaticity of fluorescence to estimate the reflectance spectrum s and the fluorescent chromaticity values E_n for all channels n . After that, the fluorescence absorption spectrum a and emission spectrum e can be recovered. Figure 4 shows an overview of the proposed method.

4.2 Reflectance Spectrum Recovery

In Section 3.3, we showed that the chromaticity of fluorescence is invariant under different illuminants. We now show how to use the illuminant-invariant chromaticity of fluorescence in conjunction with basis functions for spectral reflectance to estimate the spectral reflectance of the scene.

According to a previous study [28], the spectral reflectance of various materials can be approximately represented by using a small number of basis functions as

$$s(\lambda) = \sum_{j=1}^J \alpha_j b_j(\lambda), \quad (12)$$

where $b_j(\lambda)$ ($j = 1, 2, \dots, J$) are the basis functions (Figure 5(a)) for spectral reflectance and α_j are the corresponding coefficients. From Equation (12), Equation (8) can be rewritten as

$$r_n^m = \sum_j \alpha_j \int c_n(\lambda) l_m(\lambda) b_j(\lambda) d\lambda = \sum_j \alpha_j q_{n,j}^m, \quad (13)$$

where $q_{n,j}^m = \int c_n(\lambda) l_m(\lambda) b_j(\lambda) d\lambda$.

We now show that the illuminant-invariant chromaticity of fluorescence makes it possible to estimate the spectral reflectance s without knowing absorption spectrum a and emission spectrum e . First note that $f_n^m = p_n^m - r_n^m = p_n^m - \sum_j \alpha_j q_{n,j}^m$. According to Equation (6), the

chromaticity value E_n^m for channel n under illumination m can be computed by

$$E_n^m = \frac{f_n^m}{\sum_t f_t^m} = \frac{p_n^m - \sum_j \alpha_j q_{n,j}^m}{\sum_t (p_t^m - \sum_j \alpha_j q_{t,j}^m)} = E_n. \quad (14)$$

By straightforward algebraic manipulation of Equation (14), we can see that

$$p_n^m = E_n \sum_t (p_t^m - \sum_j \alpha_j q_{t,j}^m) + \sum_j \alpha_j q_{n,j}^m = p_n^m(\alpha, \mathbf{E}), \quad (15)$$

where α is the set of coefficients α_j ($j = 1, 2, \dots, J$) and \mathbf{E} is the set of chromaticity values E_n ($n = 1, 2, 3$), and $p_n^m(\alpha, \mathbf{E})$ is the parameterization of p_n^m . Then instead of minimizing Equation (11), we can minimize

$$G(\alpha, \mathbf{E}) = \sum_m \sum_n \|p_n^m - \hat{p}_n^m(\alpha, \mathbf{E})\|_2^2, \quad (16)$$

where $\hat{p}_n^m(\alpha, \mathbf{E})$ is called the estimated parameterization of p_n^m . Equation (16) shows that coefficients α and chromaticity \mathbf{E} can be estimated in place of s , \mathbf{a} , and \mathbf{e} .

The parameters α and \mathbf{E} need to be chosen to minimize the error function in Equation (16). Determining α would allow for recovering the spectral reflectance s according to Equation (12). Finding \mathbf{E} would provide us with the fluorescent chromaticity which will be used in later steps to determine the fluorescence spectral components.

We propose a simple and effective method for estimating parameters α and \mathbf{E} using alternating iterations to converge upon a solution. We first initialize the fluorescent chromaticity \mathbf{E} and denote it as $\hat{\mathbf{E}}$. A more detailed discussion on the initialization of \mathbf{E} can be found in Section 4.5. We then solve for α as

$$\hat{\alpha} = \arg \min_{\alpha} \sum_m \sum_n \|p_n^m - \hat{p}_n^m(\alpha, \hat{\mathbf{E}})\|_2^2. \quad (17)$$

One way to solve Equation (17) is to find α such that $p_n^m = \hat{p}_n^m(\alpha, \hat{\mathbf{E}})$. Then rearranging terms in the equation, we can get

$$y_n^m = \sum_j \alpha_j w_{n,j}^m, \quad (18)$$

where

$$\begin{aligned} y_n^m &= p_n^m - \hat{E}_n \sum_t p_t^m, \\ w_{n,j}^m &= q_{n,j}^m - \hat{E}_n \sum_t q_{t,j}^m. \end{aligned} \quad (19)$$

Equation (18) can be solved for all m and n in matrix form by finding the vector $\alpha = [\alpha_1, \dots, \alpha_J]^T$ such that

$$\mathbf{y} = \mathbf{W}\alpha, \quad (20)$$

where $\mathbf{y} = [y_1^1, y_2^1, y_3^1, \dots, y_1^M, y_2^M, y_3^M]^T$, is a $3M \times 1$ vector and \mathbf{W} is a $3M \times J$ matrix where $W_{3(m-1)+n,j} = w_{n,j}^m$.

In our system, we actually have $2M$ independent equations because chromaticity is uniquely expressed in only 2 values. We choose M , such that $2M > J$,

so the problem of estimating coefficients α is over-determined. We adopted the constrained minimization method employed in Park *et al.* [29] with a non-negative constraint on the reconstructed reflectance spectrum and use the second derivative of the reflectance spectrum with respect to λ as a smoothness constraint,

$$\begin{aligned} \hat{\alpha} &= \arg \min_{\alpha} \left\{ \|\mathbf{y} - \mathbf{W}\alpha\|_2^2 + \mu_r \int \left(\frac{\partial^2 s(\lambda)}{\partial \lambda^2} \right)^2 d\lambda \right\}, \\ \text{s.t. } & \mathbf{B}\alpha \geq 0 \quad \text{for all } \lambda, \end{aligned} \quad (21)$$

where μ_r is a weight for the constraint term and is set to be 1 in our experiments. \mathbf{B} 's columns are the reflectance spectral basis vectors b_j .

Given α estimation, \mathbf{E} can be estimated by minimizing the same error function in Equation (16) with the constraint that $\sum_n E_n = 1$. After several alternating iterations between estimating α and \mathbf{E} , we converge upon a solution where α and \mathbf{E} are well estimated. With α estimated, spectral reflectance s can be reconstructed by Equation (12).

4.3 Fluorescence Absorption Spectrum Recovery

Using the obtained spectral reflectance s and Equation (7), the appearance of the fluorescent component under the m -th illuminant is computed as $f_n^m = p_n^m - r_n^m$ so we describe how the fluorescence spectral components can be estimated given f_n^m .

Previous work has also shown that absorption spectra can be well represented by basis functions [5]. In our investigation, we have found that a large collection of absorption spectra from the McNamara and Boswell Fluorescence Spectral Dataset [26] can be well represented using 9 principal components. In our method, we use 9 principal components to describe the fluorescence absorption spectrum, as shown in Figure 5(b). Thus our observed absorption spectrum can be expressed as a linear combination of basis vectors

$$a(\lambda) = \sum_{i=1}^9 \beta_i v_i(\lambda), \quad (22)$$

where $v_i(\lambda)$ ($i = 1, \dots, 9$) is the i -th basis vector at wavelength λ and β_i is the corresponding coefficient. From Equations (3) and (22) the fluorescent component f_n^m can be described as

$$\begin{aligned} f_n^m &= D_n \sum_i \beta_m \int l_m(\lambda) v_i(\lambda) d\lambda \\ &= D_n \sum_i \beta_m h_i^m \\ &= \gamma E_n \sum_i \beta_m h_i^m, \end{aligned} \quad (23)$$

where $h_i^m = \int l_m(\lambda) v_i(\lambda) d\lambda$ and $\gamma = \sum_{t=1}^3 D_t$.

E_n was determined from Section 4.2 so it can be used to recover the fluorescence absorption spectrum by

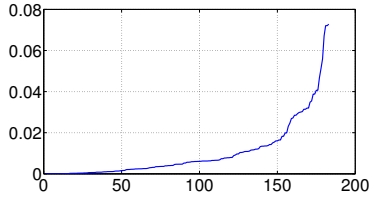


Fig. 6: All test errors sorted in ascending order. 69% of cases were below the average error of 0.01.

estimating the coefficients β_i as

$$\hat{\beta} = \arg \min_{\beta} \sum_m \sum_n \|f_n^m - \gamma E_n \sum_i \beta_i h_i^m\|_2^2. \quad (24)$$

Similar to Equation (21), this is solved with a regularization term as

$$\hat{\beta} = \arg \min \left\{ \|\mathbf{f} - \mathbf{H}\beta\|_2^2 + \mu_a \int \left(\frac{\partial^2 a(\lambda)}{\partial \lambda^2} \right)^2 d\lambda \right\},$$

s.t. $\mathbf{V}\beta \geq 0$ for all λ , (25)

where $\mathbf{f} = [f_1^1, \dots, f_3^M]^T$, is a $3M \times 1$ vector, $\beta = \gamma[\beta_1, \dots, \beta_9]^T$ is a 9×1 coefficient vector, and \mathbf{H} is a matrix where $\mathbf{H}_{3(m-1)+n,i}^m = h_i^m E_n$. \mathbf{V} is a matrix whose columns are the absorption spectral basis vectors. γ is just a scale factor that does not affect the estimated shape of the fluorescence absorption spectrum. Note that our method operates on pixels independently so γ is different for each pixel and serves to preserve the relative scale differences between pixels in a scene. μ_r is a weight for the constraint term and is set to be 1 in the experiments. With the calculated results by Equation (25), the fluorescence absorption spectrum can be recovered by Equation (22).

4.4 Fluorescence Emission Spectrum Recovery

In our system, we use an RGB camera to capture the scene and only have 2 values for the fluorescent chromaticity \mathbf{E} to recover the emission spectrum. Estimating an entire emission spectrum from only 2 values is a challenging problem but we have devised a data driven method that is effective. We observe the emission spectra in the McNamara and Boswell Fluorescence Spectral Dataset, and find most of them have similar bell shapes (see Figure 7 for examples) but with different widths and peaks at different wavelengths, which is different from reflectance spectra that can be distributed over the entire visible spectrum (see Figure 10(a) for examples). Due to the restricted types of shapes exhibited by emission spectra, we have found that similar emission chromaticities generally map to similar emission spectra. This is because these restricted types of shapes reduce the possibility of metamerism between the fluorescent chromaticities and emission spectra.

This makes it possible to determine the corresponding emission spectrum to a given fluorescent chromaticity by performing a simple procedure. We use the known camera spectral sensitivity and integrate it with each

fluorescence emission spectrum in the dataset to obtain the corresponding chromaticity for each fluorescence emission. Then, we compare the estimated fluorescent chromaticity \mathbf{E} with the fluorescent chromaticities from the dataset. The dataset emission spectrum's chromaticity with the lowest sum square error to the estimated fluorescent chromaticity \mathbf{E} is then chosen as \mathbf{E} 's emission spectrum.

To test the effectiveness of our method, we conducted tests on the McNamara and Boswell Fluorescence Spectral Dataset. We first chose a subset of materials such that the emission and absorption spectra were both present in the visible spectrum (400 - 700 nm).² This resulted in a collection of 183 materials. We then tested our method using leave-one-out cross-validation on the 183 emission spectra. In each case, the error between the estimated emission spectrum and its ground truth was computed using the mean root square error, $\sqrt{\sum_{\lambda} (e^{gt}(\lambda) - e^{es}(\lambda))^2 / d}$, where d is the length of the visible spectrum, $e^{gt}(\lambda)$ is the ground truth emission spectrum and $e^{es}(\lambda)$ is the estimated emission spectrum. Before computing the errors, the estimation and ground truth were also normalized for scale by setting the maximum value of each emission spectrum to be 1.

In our results, we found an average error of 0.01. See Figure 6 for a plot of all the errors for the 183 estimated emission spectra. We found that 69% of cases were below the average error of 0.01. Thus our results indicate that the majority of materials fit our assumption and emission spectra are accurately estimated as can be seen in Figure 7. In the 183 materials, 96% of the cases had an error of less than 0.04. We can see from Figure 7(d) that an error of 0.04 is quite reasonable. We also show our worst case error in Figure 7(e). These results show that there were some high error cases that violated our assumption but these only constituted a small set.

4.5 Fluorescent Chromaticity Initialization

Equation (10) is a nonconvex function due to bilinear correlation between the reflectance spectrum s and fluorescent chromaticity \mathbf{E} . In practice, we use a standard alternating minimization scheme to solve this problem as described in Section 4.2. To estimate the reflectance spectrum, we need to initialize the chromaticity \mathbf{E} of the fluorescent component first.

To demonstrate the effectiveness of this alternating minimization scheme for our method, we test our method under different possible initialization values for \mathbf{E} by exhaustively trying different values for chromaticity and running our alternating iterations to see what kinds of chromaticity values would be converged upon. For the types of initializations tested, we choose a dense and uniformly distributed set of initializations for \mathbf{E}

² We chose this subset because our experimental setup is currently focused on imaging in the visible spectrum. Although conceptually, our methods would extend to non-visible wavelengths as well.

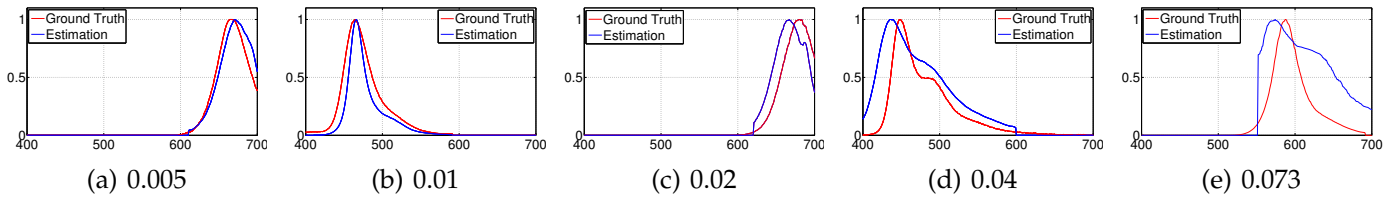


Fig. 7: Examples of estimated emission spectra and their mean root square errors.

TABLE 1: Average and standard deviations of the converged upon estimated chromaticities under all 66 initializations of \mathbf{E} are shown in the second and third columns. The 66 initializations are densely and uniformly distributed in the space of possible initializations of \mathbf{E} . The low standard deviations indicate our estimation method is robust to different initializations of \mathbf{E} .

Sheets	Average Chromaticity	Standard Deviation	Ground Truth Truth
Pink	(0.61, 0.19)	(0.01, 0.00)	(0.61, 0.20)
Green	(0.15, 0.64)	(0.01, 0.02)	(0.16, 0.64)
Orange	(0.56, 0.32)	(0.02, 0.02)	(0.56, 0.31)
Red	(0.61, 0.21)	(0.00, 0.00)	(0.61, 0.20)
Yellow	(0.19, 0.62)	(0.01, 0.03)	(0.19, 0.62)

from the space of possible chromaticities. For each channel n , we set E_n to values from 0 to 1 in increments of 0.1 with the constraint that $E_1 + E_2 + E_3 = 1$. This amounted to 66 initializations³ for the (E_1, E_2, E_3) values.

Table 1 shows average estimated chromaticities and their standard deviations for all 66 initializations for the 5 fluorescent sheets on the color wheel in Figure 4. We found the averages shown in Table 1 to be close to the ground truth chromaticities. In addition, the standard deviations of the 66 initializations is very small for all the fluorescent sheets tested. This indicates that our estimation method is very robust to the choice of initialization values of \mathbf{E} .

4.6 Summary of the Algorithm

We exploit the unique property of fluorescence that the chromaticity of fluorescent emissions are invariant under different illuminants to simplify our optimization in Equation (10) into 3 sub-problems: reflectance spectrum s recovery, fluorescence absorption spectrum a recovery, and fluorescence emission spectrum e recovery. However, the optimization problem in Equation (16) for reflectance spectrum s recovery is also challenging due to its nonconvexity from the bilinear correlation between s and \mathbf{E} . The global minimum for Equation (16) can be found via a two-dimensional exhaustive search but this would be extremely slow. Meanwhile, using certain local optimization methods would require a reasonable initialization. In practice, we minimize Equation (16) via a standard alternating minimization scheme with an initialized fluorescent chromaticity \mathbf{E} . In Section 4.5, we

3. When E_1 is initialized to 0, E_2 will have 11 selections from 0 to 1 in 0.1 increments, E_3 will be $1 - E_1 - E_2$. When E_1 is initialized as 0.1, E_2 will have 10 selections from 0 to 0.9 in 0.1 increments, and so on. So there are $(11 + 10 + \dots + 1) = 66$ possible initializations.

can see that the standard deviations of the recovered fluorescent chromaticities \mathbf{E} under different initializations are very small for all the fluorescent sheets tested, which show that our method converges well under different initializations and tends to avoid local minima.

In practice, the maximum number of iterations for the alternating minimization procedure was chosen to be 10 in all experiments. We exhaustively initialize fluorescent chromaticities \mathbf{E} using the 66 possible settings and choose the one that minimizes $\sum_n \sum_m \|p_n^m - p_n^m(\alpha, \mathbf{E})\|$ as the estimated result for each pixel. The proposed method can be seen in Algorithm 1.

Algorithm 1: Reflectance, fluorescence absorption and emission spectra estimation

Input : Images captured under varied illuminants
Output: Recovered reflectance, fluorescence absorption and emission spectra for all pixels

- 1 **for** $t = 1, 2, \dots, T$ **do**
 - 2 Set the fluorescent chromaticity \mathbf{E} to the t^{th} initialization;
 - 3 **for** $h = 1, 2, \dots, H$ **do**
 - 4 Estimate the reflectance spectrum s via Equations (21) and (12);
 - 5 Update the chromaticity of the fluorescent component \mathbf{E} ;
 - 6 **end**
 - 7 Estimate the absorption spectrum a via Equations (25) and (22);
 - 8 **end**
 - 9 Select the best estimated s , a and \mathbf{E} , to minimize Equation (10) from all T estimations;
 - 10 Estimate the emission spectrum e by the fluorescent chromaticity \mathbf{E} according to Section 4.4.
-

5 RESULTS AND ANALYSIS

The performance of our method was tested by using images taken by a CCD camera (SONY DXC-9000) under varied illuminants. The camera spectral sensitivity is shown in Figure 8. The types of illuminants used were 9 colored lights ranging from blue to red in the visible spectrum as shown in Figure 9(a), which were produced by a Nikon Equalized Light Source (ELS) in our experiments. The camera spectral sensitivity was calibrated by using a white target and narrowband illuminants produced by a Nikon Equalized Light Source (ELS). We used a PR-670 SpectraScan Spectroradiometer to collect ground truth spectra and illuminant spectra.

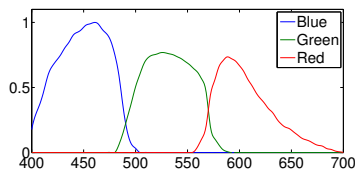


Fig. 8: Camera spectral sensitivity used in our experiments.

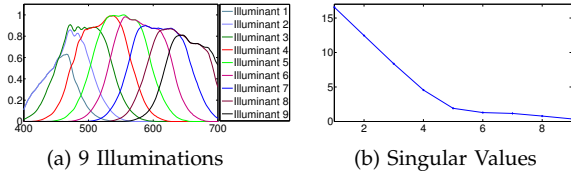


Fig. 9: The spectra of our 9 colored illuminants and corresponding singular values.

5.1 Recovery of Spectra

We first evaluate the accuracy of the recovered spectral reflectance and fluorescence absorption and emission spectra of all 5 fluorescent sheets on the color wheel of Figure 4. We capture the ground truth spectra of all these fluorescent sheets by using the method described in Section 3.2. Figure 10 shows the recovered spectral reflectance and fluorescence absorption and emission spectra of all 5 fluorescent sheets. Compared with the ground truth, we can see that the recovered spectral reflectance (Figure 10(a)), absorption spectra (Figure 10(b)) and emission spectra (Figure 10(c)) of all fluorescent sheets approximate the ground truth well. All these results demonstrate that our method can effectively recover spectral reflectance and fluorescence absorption and emission spectra by only using an RGB camera under multiple illuminations.

We also compared our method against state-of-art work [6], which requires a hyperspectral camera and specialized illuminants. In Figure 11, we can see that our method and [6] both approximate the ground truth well. It shows that our method can achieve competitive results with [6] and effectively recover all spectra for reflective-fluorescent scenes by using lower costing equipment.

5.2 Relighting Results

Since our method is able to recover the full spectral reflectance, fluorescence absorption, and fluorescence emission spectra for an entire reflective-fluorescent scene, the scenes can be separated into reflective and fluorescent components, and relit under different illuminations, as shown in Figures 12-15.

Figure 12 shows the separation of reflectance and fluorescence for a reflective-fluorescent scene as well

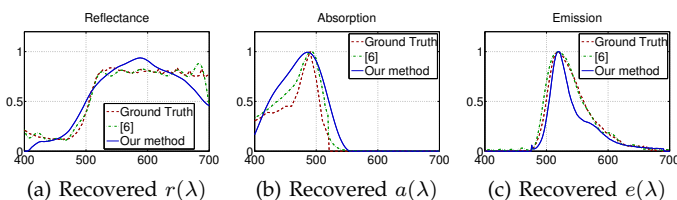


Fig. 11: Comparison between [6] and our method on fluorescent yellow sheet.

as relighting results with different initializations of the fluorescent chromaticity. In Figures 12(c) and (e) we can see the recovered reflective and fluorescent components. In the scene, the notebook on the left only has ordinary reflectance so its colors in the recovered reflective component (Figure 12(c)) are the same as those seen under white light (Figure 12(a)).

The ground truth for the color wheel scene under the 5 illuminants can be seen in Figure 12(b) and the corresponding relighting results (Figure 12(f) (h) (j) and (l)) are rendered by the recovered spectra s , a , and e under different initialization conditions for fluorescent chromaticities \mathbf{E} . Figure 12(f) shows the best results for each pixel chosen from the 66 possible initializations described in our exhaustive tests in Section 4.5. We can see that these relighting results (Figure 12(f)) approximate the ground truth well (Figure 12(b)).

To further demonstrate that our method is robust to the fluorescent chromaticity initializations, we also show the relighting results (Figure 12(h) (j) and (l)) under 3 other initialized fluorescent chromaticities, which are the image captured under near UV light (Figure 12(g), it is a close approximation to observing the ground truth chromaticity), average image from the 9 input color images (Figure 12(i), it is similar to the image captured under white light), and the flat chromaticity $(1/3, 1/3, 1/3)$ for the R, G, and B channels (Figure 12(k)), respectively. We can see that these relighting results (Figure 12 (h) (j) and (l)) are close to the ground truth (Figure 12(b)). In fact, all the visual relighting results (Figure 12(f) (h) (j) and (l)) are virtually indistinguishable and match the ground truth well.

When the scene is relit without considering fluorescent effects in the scene (Figure 12(d)), this leads to many fluorescent materials appearing as black, especially under blue-green light (the first column in Figure 12(d)). For the parts of the image that are not black, we can only observe the colors that are present in the illuminant. For example, under blue-green light, Figure 12(d) only shows blue and green colors.

Figures 13-15 show additional separation of reflectance and fluorescence on 3 other fluorescent scenes and their relighting results. We found all relighting results under different initializations to be nearly identical so we only show the relighting results from the best estimated spectra under the 66 initializations for these 3 scenes. The relighting results were all close to the ground truth and the fluorescent parts were well separated from the reflective parts. For example, Figure 13 shows highly fluorescent objects such as the fluorescent pen at the bottom. In the reflectance only image (Figure 13(c)), those objects are very dark while they are very bright in the fluorescence only image (Figure 13(d)). Similar results can be observed from the other scenes. These additional results on real scenes show that our method is robust to different types of materials and initialization conditions in the optimization.

We also quantitatively evaluate the errors between

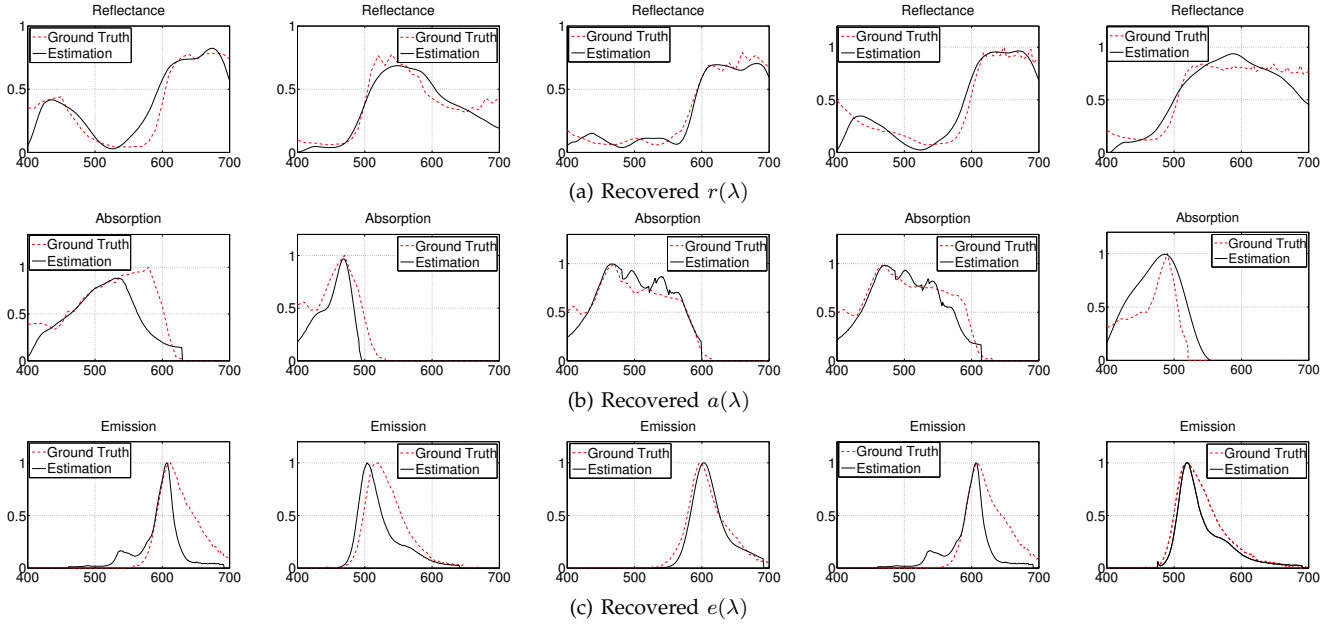


Fig. 10: Recovered reflectance $r(\lambda)$, fluorescence absorption $a(\lambda)$ and emission $e(\lambda)$ spectra of the 5 fluorescent sheets in the color wheel of Figure 4. The recovered results for 5 fluorescent sheets from top to bottom in the color wheel are shown from from in the columns from left to right.

TABLE 2: The errors between the ground truth and the relit results. “R Only” means only reflectance was considered. The “R+F” means reflectance and fluorescence were considered. “R+F 1”, “R+F 2”, “R+F 3” and “R+F 4” are the errors between the ground truth and the relighting results under different initialized fluorescent chromaticities, which are respectively, the exhaustive 66 initializations, the image captured under near UV light, average image from input 9 images, and the flat chromaticity $(1/3, 1/3, 1/3)$ for the R, G, and B Channels. “Max” and “Min” correspond to the maximum and minimum errors under 5 different illuminants, respectively .

Scene	R Only		R+F 1		R+F 2		R+F 3		R+F 4	
	Min	Max								
Color Wheel	0.3434	0.4696	0.0265	0.0404	0.0273	0.0481	0.0290	0.0502	0.0268	0.0490
Cup	0.2286	0.3007	0.0220	0.0330	0.0288	0.0371	0.0220	0.0372	0.0222	0.0379
Train	0.3336	0.6381	0.0333	0.0670	0.0362	0.0679	0.0347	0.0672	0.0344	0.0682
Gun	0.3411	0.6376	0.0283	0.0522	0.0302	0.0543	0.0300	0.0571	0.0298	0.0547

the virtual relighting of all these 4 reflective-fluorescent scenes and their ground truth. We computed errors between the ground truth and the relit results as

$$\sqrt{\frac{\sum_n (p_n^{gt} - p_n^{re})^2}{\sum_n (p_n^{gt})^2}} \quad (26)$$

where p_n^{gt} is the ground truth (corresponding images in Figures 12-15(b)) and p_n^{re} is the relighting result. Table 2 shows the maximum and minimum errors for 4 scenes under 5 illuminants and under different initializations. “R Only” means only reflectance was considered. The “R+F” means reflectance and fluorescence were both considered. “Max” and “Min” correspond to the maximum and minimum errors under the 5 different illuminants, respectively. “R+F 1”, “R+F 2”, “R+F 3” and “R+F 4” are the errors between the ground truth and the relighting results under different initialized fluorescent chromaticities, which are respectively, from the 66 possible initializations in our exhaustive test, the image captured under near UV light, average image from the 9 input images in our method, and the flat chromaticity $(1/3, 1/3, 1/3)$ for R, G, and B channels. We can see that

the errors are large when only reflectance is considered. When fluorescence is considered, the errors are small and show that the predicted colors are very close to their ground truth images. The errors for relighting results from the 4 fluorescent chromaticity initializations strategies are also very similar. The “R+F 1” with he best estimated spectra from the 66 initializations is only a little better than other results. This slightly better accuracy is visually indistinguishable in the relit images (Figure 12). These quantitative results reconfirm that our method is robust and converges well under different fluorescent chromaticity initializations.

6 DISCUSSION ON ILLUMINANTS

The illuminants used in our experiments can be produced by LEDs or other light sources. For testing purposes, we employed a programmable light source (Nikon ELS) to produce the 9 colored lights in our experiments. To be effective, the light sources need to satisfy 2 conditions:

First, the spectra of all the illuminants should be linearly independent as images captured under linearly

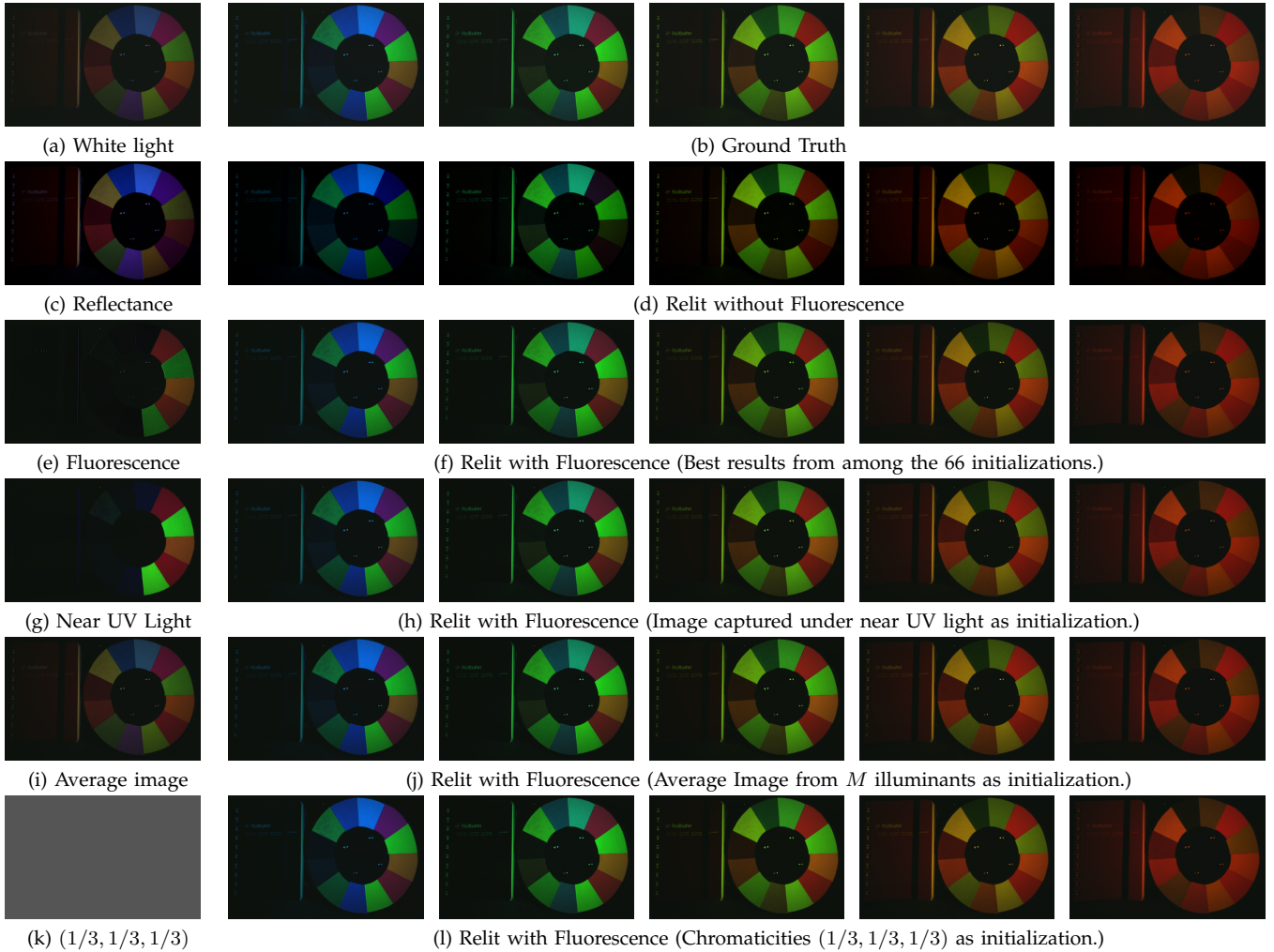


Fig. 12: Relighting results for the fluorescent color wheel.

correlated illuminants cannot provide new information. In Equation (9), if the spectrum of one illuminant can be described as a linear combination of 2 other illuminants as

$$l_3(\lambda) = \tau_1 l_1(\lambda) + \tau_2 l_2(\lambda), \quad (27)$$

then substituting Equation (27) into Equation (9), the intensity for the n^{th} channel of the reflective-fluorescent scene can be represented as

$$\begin{aligned} p_n^3 &= \int c_n(\lambda) l_3(\lambda) s(\lambda) d\lambda \\ &+ \left(\int l_3(\lambda') a(\lambda') d\lambda' \right) \int c_n(\lambda) e(\lambda) d\lambda \\ &= \int c_n(\lambda) (\tau_1 l_1(\lambda) + \tau_2 l_2(\lambda)) s(\lambda) d\lambda \\ &+ \left(\int (\tau_1 l_1(\lambda') + \tau_2 l_2(\lambda')) a(\lambda') d\lambda' \right) \int c_n(\lambda) e(\lambda) d\lambda \\ &= \tau_1 p_n^1 + \tau_2 p_n^2 \end{aligned} \quad (28)$$

This means that the image captured under illuminant l_3 can be expressed as a linear combination of the images captured under illuminants l_1 and l_2 . The third image captured under l_3 would thus provide no additional

information beyond that found in the images captured under l_1 and l_2 .

A second requirement is that the spectra of all illuminants combined should, as much as possible, uniformly cover the visible spectrum. If some range of wavelengths were not covered by any illuminants, it would affect the recovery of reflectance and absorption spectra in that range. This is because we do not know in advance where along the spectrum the fluorescence absorption spectra will be present. If the illuminants span the entire visible spectrum, we can assure that our method would be robust to different materials and their different spectra.

The 9 illuminants (Figure 9(a)) used in our experiments are evenly distributed in the spectral domain and cover all visible wavelength. The linear independence of these 9 illuminant spectra can be evaluated by their singular values and condition number. Their singular values are shown in Figure 9(b) and their condition number is 44.57. The condition numbers of the W term in Equation (21) and H term in Equation (25) are 45.95 and 74.06 under these illuminants, respectively. In the W and H terms, the bases and RGB camera spectral sensitivity are considered and shown in Figures 5 and

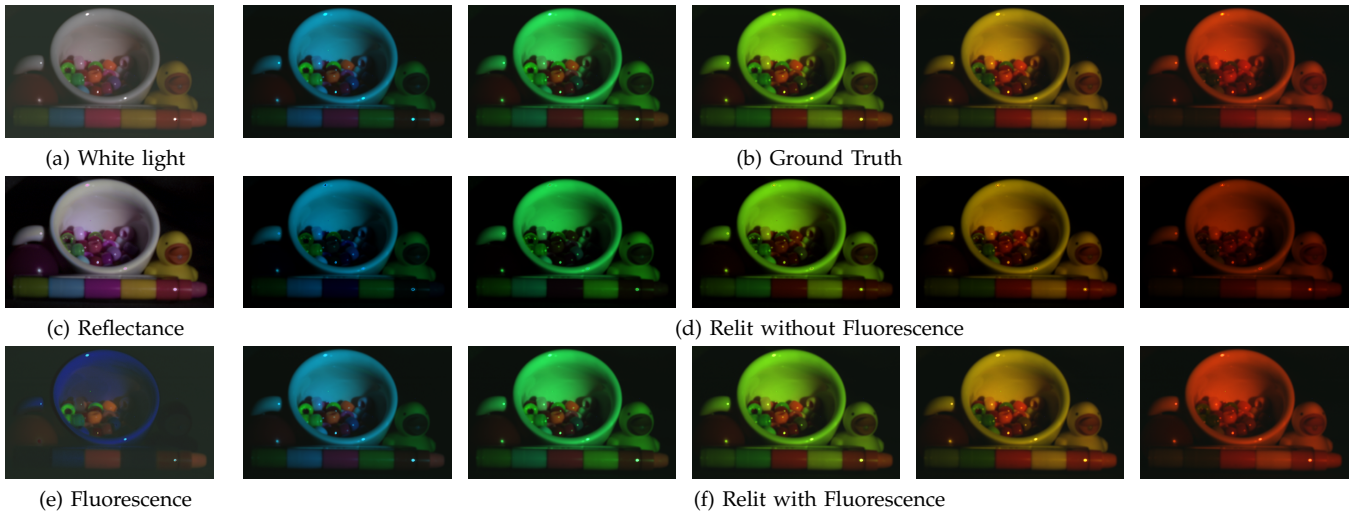


Fig. 13: Relighting results for the fluorescent cup scene.

8, respectively. The closer the condition number is to 1, the stronger the linear independence. Our results indicate that this level of linear independence of light sources is good enough to provide accurate estimation of reflectance and fluorescence absorption spectra.

In our experiments, we produced the illuminants using a programmable light source. We also evaluated our approach by performing an analysis using the spectra of off-the-shelf LEDs. In Figure 16, the spectra of these 9 off-the-shelf LED light sources and their corresponding singular values are shown. These light sources also satisfy our requirements for effective imaging of all spectral components. The condition number for these 9 illuminants is 9.50, which is much less than the 44.57 condition number of our original illuminants. The condition numbers of the W and H terms are 15.92 and 22.57 under these illuminants, respectively. The condition numbers of W and H under the off-the-shelf LED light sources are also much lower than those of the original illuminants used in our experiments, so theory shows we can obtain better experimental results under these LEDs than with the illuminants produced by our programmable light source.

To evaluate our method under our illuminants and off-the-shelf LED light sources, we first randomly selected one color from the 16 color patches on the Macbeth ColorChecker as the reflectance spectrum. As for the absorption and emission pair, we randomly selected one pair from the fluorescence spectral dataset [26] from among the 183 materials used in this paper. All spectra were normalized such that the maximum value was 1 for each spectrum. We then simulated our method on these spectra under our illuminants and the off-the-shelf LED light sources. After the simulation, we calculated the errors between the recovered spectra and the ground truth like in Section 4.4. The mean errors for the recovered reflectance and fluorescence absorption spectra are 0.012 and 0.007 under our illuminants, while the mean errors are 0.009 and 0.007 under off-the-shelf

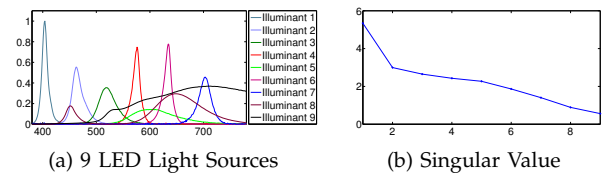


Fig. 16: The spectra of off-the-shelf LED light sources and corresponding singular values.

LED lights. We can see that the mean errors from using these two sets of illuminants are close. Therefore, our method can be directly applied using off-the-shelf light sources.

7 CONCLUSION AND LIMITATIONS

In this paper, we presented a method to simultaneously recover the reflectance and fluorescence absorption and emission spectra of an entire scene by using RGB images under varied illuminants. Making use of the illuminant-invariant chromaticity of fluorescence, our method is capable of estimating the reflectance spectrum and chromaticity of the fluorescent component. Moreover, the fluorescence absorption and emission spectra are estimated accurately by exploiting the basis representation of absorption spectra and a strong correlation between fluorescent chromaticity and emission spectra, respectively. The effectiveness of the proposed method was successfully demonstrated with experiments on real data taken under varied illuminants. In addition, the recovered spectra were used to accurately relight scenes.

There are still some limitations in our method that are worth further investigation in the future. Estimating all three spectra from RGB values observed under different illuminants is a difficult task. To overcome these difficulties, we employed 9 colored illuminants in our method. This is time consuming and makes it impractical to directly extend our method to moving fluorescent scenes. To solve this problem, we will investigate how we might relax our constraints to reduce the number

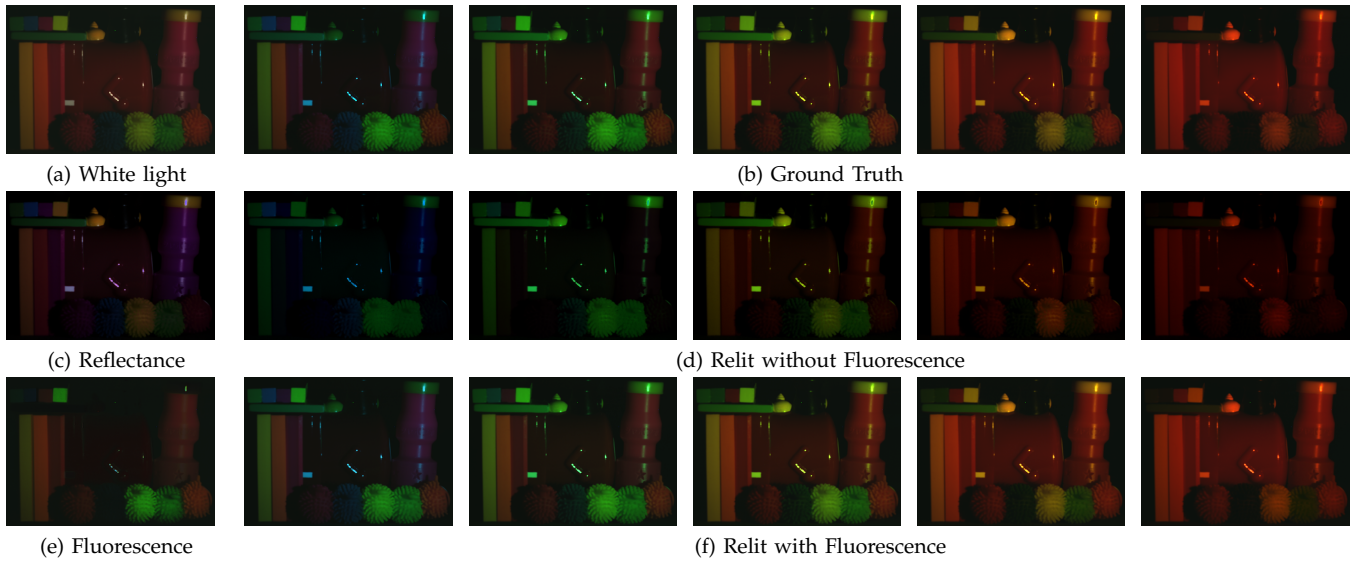


Fig. 14: Relighting results for the fluorescent train scene.

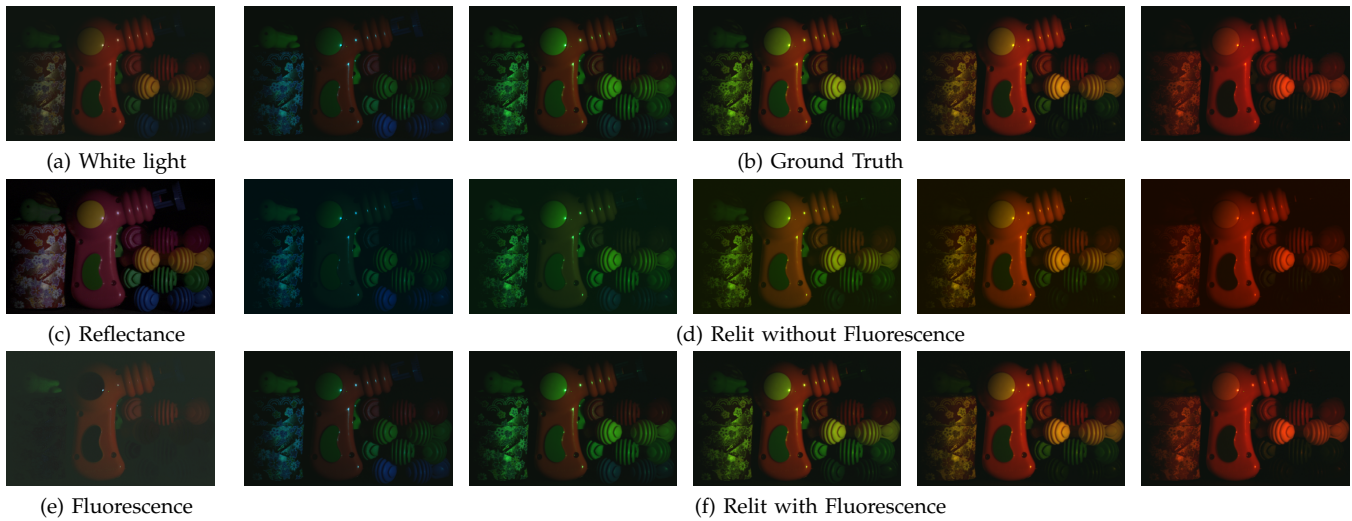


Fig. 15: Relighting results for the fluorescent toy gun scene.

of required input images. In addition, we can also use a high speed camera to capture multiple images in a short amount of time. We also required a dataset for emission spectra estimation. One of the extensions of our approach will be to employ multi-channel cameras (e.g. 5 channels) with more narrowband sensitivities and investigate how we can estimate emission spectra without relying on a dataset. Another issue is that our method needs to be calibrated to the camera spectral sensitivity and the illuminant spectra in advance. There are existing methods that can be used to calibrate camera spectral sensitivity [1], [30] and illuminants [16]. In the future, it is worth investigating how we can estimate all reflectance, absorption, and emission spectra under unknown camera spectral sensitivity or illuminant spectra by combining those existing methods as well as considering the fluorescent property for camera spectra sensitivity and illuminant recovery.

ACKNOWLEDGMENTS

This research was supported in part by the Ministry of Education, Science, Sports and Culture Grant-in-Aid for Scientific Research on Innovative Areas.

REFERENCES

- [1] S. Han, Y. Matsushita, I. Sato, T. Okabe, and Y. Sato, "Camera spectral sensitivity estimation from a single image under unknown illumination by using fluorescence," in *Proc. of IEEE Conference on Computer Vision and Pattern Recognition (CVPR)*, 2012.
- [2] I. Sato, T. Okabe, and Y. Sato, "Bispectral photometric stereo based on fluorescence," in *Proc. of IEEE Conference on Computer Vision and Pattern Recognition (CVPR)*, 2012.
- [3] T. Treibitz, Z. Murez, B. G. Mitchell, and D. Kriegman, "Shape from fluorescence," in *Proc. of European Conference on Computer Vision (ECCV)*, 2012, pp. 292–306.
- [4] M. B. Hullin, M. Fuchs, I. Ihrke, H.-P. Seidel, and H. P. A. Lensch, "Fluorescent immersion range scanning," *ACM Trans. on Graph. (Proc. of SIGGRAPH)*, vol. 27, pp. 87:1–87:10, 2008.
- [5] A. Lam and I. Sato, "Spectral modeling and relighting of reflective-fluorescent scenes," in *Proc. of IEEE Conference on Computer Vision and Pattern Recognition (CVPR)*, 2013.

[6] Y. Fu, A. Lam, I. Sato, T. Okabe, and Y. Sato, "Separating reflective and fluorescent components using high frequency illumination in the spectral domain," in *Proc. of International Conference on Computer Vision (ICCV)*, 2013.

[7] G. Johnson and M. Fairchild, "Full-spectral color calculations in realistic image synthesis," *IEEE Computer Graphics and Applications*, vol. 19, pp. 47–53, Aug. 1999.

[8] C. Zhang and I. Sato, "Image-based separation of reflective and fluorescent components using illumination variant and invariant color," *IEEE Trans. Pattern Analysis and Machine Intelligence (PAMI)*, vol. 35, no. 12, pp. 2866–2877, Dec. 2013.

[9] F. W. D. Rost, *Fluorescence Microscopy*. Cambridge University Press, 1992.

[10] J. R. Lakowicz, *Principles of Fluorescence Spectroscopy*. Springer, 2006.

[11] J. E. Leland, N. L. Johnson, and A. V. Arcchi, "Principles of bispectral fluorescence colorimetry," in *Proc. SPIE*, vol. 3140. SPIE, 1997, pp. 76–87.

[12] S. Tominaga, "Multichannel vision system for estimating surface and illumination functions," *JOSA A*, vol. 13, no. 11, pp. 2163–2173, 1996.

[13] J.-I. Park, M.-H. Lee, M. D. Grossberg, and S. K. Nayar, "Multispectral imaging using multiplexed illumination," in *Proc. of International Conference on Computer Vision (ICCV)*, 2007, pp. 1–8.

[14] C. Chi, H. Yoo, and M. Ben-Ezra, "Multi-spectral imaging by optimized wide band illumination," *International Journal of Computer Vision (IJCV)*, vol. 86, no. 2-3, pp. 140–151, 2010.

[15] S. Han, I. Sato, T. Okabe, and Y. Sato, "Fast spectral reflectance recovery using DLP projector," in *Proc. of Asian Conference on Computer Vision (ACCV)*, 2010, pp. 323–335.

[16] J. Jiang and J. Gu, "Recovering spectral reflectance under commonly available lighting conditions," in *IEEE Computer Society Conference on Computer Vision and Pattern Recognition Workshops (CVPRW)*, 2012.

[17] B.-K. Lee, F.-C. Shen, and C.-Y. Chen, "Spectral estimation and color appearance prediction of fluorescent materials," *Optical Engineering*, vol. 40, pp. 2069–2076, 2001.

[18] K. Barnard, "Color constancy with fluorescent surfaces," in *CIC, Proceedings of the IS&T/SID Color Imaging Conference*, 1999.

[19] A. Wilkie, A. Weidlich, C. Larboulette, and W. Purgathofer, "A reflectance model for diffuse fluorescent surfaces," in *International conference on Computer graphics and interactive techniques*, 2006, pp. 321–331.

[20] M. B. Hullin, J. Hanika, B. Ajdin, H.-P. Seidel, J. Kautz, and H. P. A. Lensch, "Acquisition and analysis of bispectral bidirectional reflectance and reradiation distribution functions," *ACM Trans. on Graph. (Proc. of SIGGRAPH)*, vol. 29, pp. 97:1–97:7, 2010.

[21] S. Tominaga, T. Horiuchi, and T. Kamiyama, "Spectral estimation of fluorescent objects using visible lights and an imaging device," in *Proceedings of the IS&T/SID Color Imaging Conference*, 2011.

[22] M. Alterman, Y. Schechner, and A. Weiss, "Multiplexed fluorescence unmixing," in *Proc. of International Conference on Computational Photography (ICCP)*, 2010.

[23] E. Fuchs, "Separating the fluorescence and reflectance components of coral spectra," *Applied Optics*, vol. 40, no. 21, pp. 3614–3621, Jul. 2001.

[24] Y. Zheng, I. Sato, and Y. Sato, "Spectra estimation of fluorescent and reflective scenes by using ordinary illuminants," in *Proc. of European Conference on Computer Vision (ECCV)*, 2014, pp. 188–202.

[25] Y. Fu, A. Lam, Y. Matsushita, I. Sato, and Y. Sato, "Interreflection removal using fluorescence," in *Proc. of European Conference on Computer Vision (ECCV)*, 2014.

[26] G. McNamara, A. Gupta, J. Reynaert, T. D. Coates, and C. Boswell, "Spectral imaging microscopy web sites and data," *Cytometry. Part A: the journal of the International Society for Analytical Cytology*, vol. 69, no. 8, pp. 863–871, 2006.

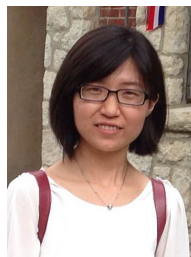
[27] "Fluorescence." [Online]. Available: <http://micro.magnet.fsu.edu/primer/lightandcolor/fluoroexcitation>

[28] J. P. S. Parkkinen, J. Hallikainen, and T. Jaaskelainen, "Characteristic spectra of munsell colors," *Journal of the Optical Society of America A*, vol. 6, no. 2, pp. 318–322, 1989.

[29] J. Park, M. Lee, M. D. Grossberg, and S. K. Nayar, "Multispectral Imaging Using Multiplexed Illumination," in *Proc. of International Conference on Computer Vision (ICCV)*, 2007.

[30] J. Jiang, D. Liu, J. Gu, and S. Susstrunk, "What is the space of spectral sensitivity functions for digital color cameras?" in *IEEE*

Workshop on Applications of Computer Vision (WACV), Jan. 2013, pp. 168–179.



Ying Fu received the B.S. degree in Electronic Engineering from Xidian University in 2009 and the M.S. degree in Automation from Tsinghua University in 2012. She joined the graduate school of information science and technology at the University of Tokyo in 2012, where she is currently a Ph.D. candidate under the supervision of Prof. Yoichi Sato. Her research interests include physics-based vision, image processing, and computational photography.



Antony Lam received the B.S. degree in Computer Science at the California State Polytechnic University, Pomona in 2004 and the Ph.D. in Computer Science at the University of California, Riverside in 2010. After working at the National Institute of Informatics, Japan, he joined the Graduate School of Science and Engineering at Saitama University as an assistant professor in 2014. His research interests are mainly in computer vision with emphasis on the areas of physics-based vision and pattern recognition.



Imari Sato received the B.S. degree in policy management from Keio University in 1994. After studying at the Robotics Institute of Carnegie Mellon University as a visiting scholar, she received the M.S. and Ph.D. degrees in interdisciplinary Information Studies from the University of Tokyo in 2002 and 2005, respectively. In 2005, she joined the National Institute of Informatics, where she is currently an associate professor. Her primary research interests are in the fields of computer vision (physics-based vision, image-based modeling) and Computer Graphics (image-based rendering, augmented reality). She has received various research awards, including IPSJ Nagao Special Researcher award (2010), The Young Scientists' Prize from The Commendation for Science and Technology by the Minister of Education, Culture, Sports, Science and Technology (2009), and Microsoft Research Japan New Faculty award (2011).



Takahiro Okabe received the B.S. and M.S. degrees in physics, and the Ph.D. degree in information science and technology from the University of Tokyo, Japan, in 1997, 1999 and 2011 respectively. After working at the Institute of Industrial Science, the University of Tokyo, he joined Kyushu Institute of Technology, Japan, as an associate professor in 2013. His research interests include computer vision, image processing, pattern recognition, and computer graphics, in particular their physical and mathematical aspects.



Yoichi Sato is a professor at Institute of Industrial Science, the University of Tokyo. He received his B.S. degree from the University of Tokyo in 1990, and his M.S. and Ph.D. degrees in robotics from School of Computer Science, Carnegie Mellon University in 1993 and 1997 respectively. His research interests include physics-based vision, reflectance analysis, image-based modeling and rendering, and gaze and gesture analysis. He served/is serving in several conference organization and journal editorial roles including IEEE Transactions on Pattern Analysis and Machine Intelligence, International Journal of Computer Vision, Computer Vision and Image Understanding, IET Computer Vision, IPSJ Journal of Computer Vision and Applications, ECCV2012 Program Co-Chair and MVA2013 General Chair.